Chirality Amplified: Long, Discrete Helicene Nanoribbons

Xiao Xiao,[1] Stephan K. Pedersen,[1,2] Daniel Aranda,[3,4] Jingjing Yang,[1] Ren A. Wiscons,[1] Michael Pittelkow,[2] Michael L. Steigerwald,[1] Fabrizio Santoro,[4*] Nathaniel J. Schuster,[1*] and Colin Nuckolls[1*]

[1]Department of Chemistry, Columbia University, New York 10027, USA. [2]Department of Chemistry, University of Copenhagen, DK-2100 Copenhagen Ø, Denmark. [3]Departamente de Quimica Fisica, Universidad de Malaga, Bulevar Louis Pasteur 31, Malaga 29010, Spain. [4]CNR-Consiglio Nazionale delle Ricerche, Istituto di Chimica dei Composti Organo Metallici (ICCOM-CNR), SS di Pisa, Area della Ricerca, via G. Moruzzi 1, I-56124 Pisa, Italy.

ABSTRACT: Here we report the synthesis of two polyhelicene frameworks consisting, from end-to-end, of 18 and 24 fused benzene rings. The latter exhibits the largest electronic circular dichroism in the visible spectrum of any molecule. These shape-persistent helical nanoribbons incorporate multiple helicenes, a class of contorted polycyclic aromatic molecules consisting of *ortho*-annulated rings. These conjugated, chiral molecules have interesting chemical, biological, and chiroptical properties; however, there are very few helicenes with extraordinary chiroptical response over a broad range of the visible spectrum–a key criterion for applications such as chiral optoelectronics. In this report, we show that coupling the polyhelicene framework with multiple perylene-diimide subunits elicits a significant chiroptic response. Notably, the molar circular dichroism increases faster than the absorptivity of these molecules as their helical axis lengthens. Computational analysis reveals the greatly amplified circular dichroism arises from exciton-like interactions between the perylene-diimide and the helicene moieties. We predict that even greater chiroptic enhancement will result from further axial elongation of these nanoribbons, which can be readily enabled via the iterative synthetic method presented herein.

Introduction

The design and synthesis of helicenes with the ability to interact with one hand of circularly polarized light with high selectivity across a broad range of wavelengths, especially in the visible range, are key to the development of future chiral materials and understanding the mechanism for chiroptic amplification.[1] The integration of chirality and π-conjugation in these helicenes provides the opportunity for a host of applications such as asymmetric catalysis,[2] chiroptical switches/sensors,[3] nonlinear optics,[4] and spin filters.[5] Helicenes are also promising building blocks for chiral electronic and optoelectronic materials[6] due to their structural diversity enabled by the development of new synthetic methodologies:[7] they can incorporate π-surfaces with various sizes[8] and chemical functionalities.[9]

Chiroptic properties are typically investigated by using electronic circular dichroism (ECD) spectroscopy.[10] Despite an interest in materials that absorb in the visible, most helicenes only exhibit strong absorbance in the ultraviolet regime, and, moreover, they in general do not exhibit intense chiroptical properties.[11] For example, in the carbo[n]helicene series (where n denotes the number of *ortho*-fused benzene rings), absorption in the visible only occurs with $n \geq 7$, and axial elongation ($n \geq 6$) elicits little change in the magnitude of ECD ($|\Delta\varepsilon|_{max}$ = ca. 300 M^{-1} cm^{-1}).[12] On the other hand, fusion of multiple helicenes into a nanographene core has been exploited extensively to

afford a variety of extended helical nanostructures, which generally do absorb in the visible range.[13] However, this approach often leads to merely comparable ECD intensity relative to that of simply one of the helicene components,[14] and only a few designs infer how ECD may be further amplified in these systems.[11] Therefore, a series of closely related molecular architectures with clear structure-function relationships needs to be established to devise broadly applicable design principles.

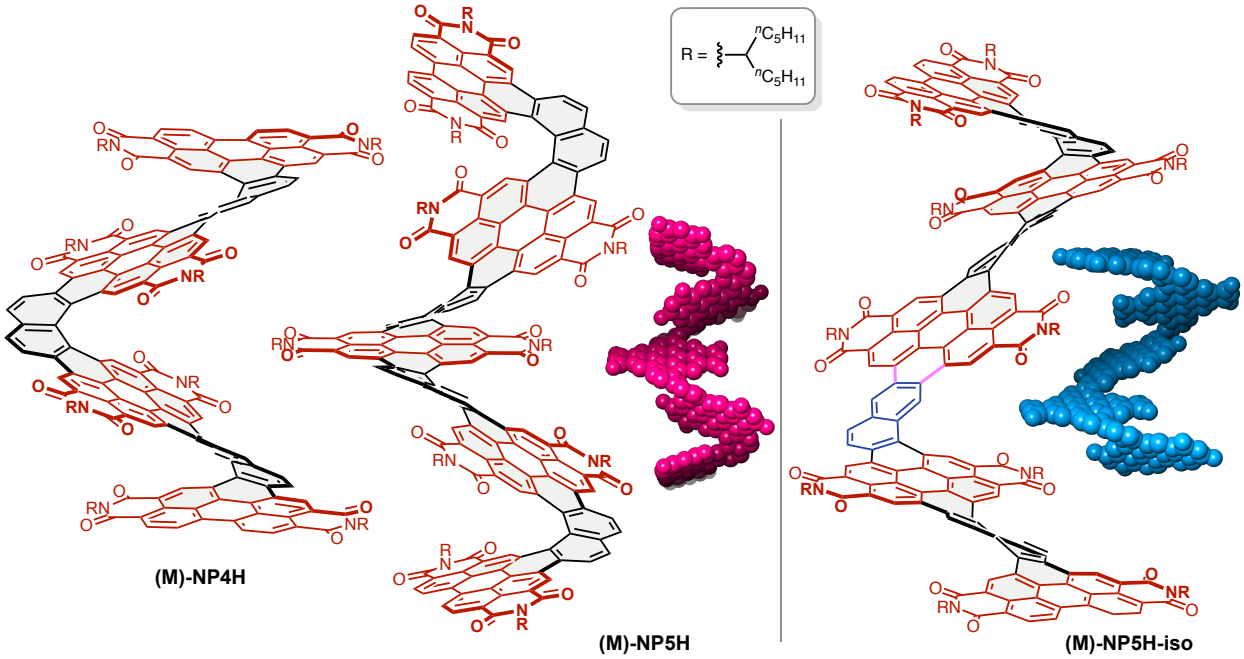

Figure 1. The structures of the **NP4H**, **NP5H**, and **NP5H-iso**. Only the left-handed helices are shown. The carbo[6]helicene and perylenediimide subunits are highlighted in grey and red, respectively.

Here we present two long and shape-persistent helicene nanoribbons, **NP4H** and **NP5H** (Figure 1), which consist of multiple [6]helicene (grey) and perylene-3,4,9,10-tetracarboxylic-diimide[15] (PDI, red) moieties. **NP5H** exhibits the largest molar ECD (> 1900 M^{-1} cm^{-1}) in the visible spectrum ever recorded for a molecule,[16] as well as high molar absorptivity and fluorescence quantum yield. **NP5H** is also one of the longest discrete helicenoid structures: its helical backbone, from one end to the other, comprises four axially fused carbo[6]helicenes (i.e., 24 benzene rings).[8,9c] In contrast to single-chromophores, multichromophoric chiral systems with proper spatial interactions between each subunit (i.e., exciton couplings) often give rise to larger ECD, especially when the chromophores are degenerate.[17] Accordingly, the many identical chromophores (e.g., PDI and [6]helicenes) in **NP4H** and **NP5H** enhance exciton-like couplings, which yield massive chiroptic amplification as compared to the shorter analogues in the **NPnH** series (i.e., **NPDH** and **NP3H** in Figure S3a, where n represents the number of PDI units).[18] Furthermore, the study of an isomeric structure of **NP5H** (i.e., **NP5H-iso** in Figure 1) suggests that a small structural defect greatly diminishes the overall ECD. Finally, density functional theory (DFT) calculations reveal the role of exciton-like couplings in enhancing the ECD, and that further axial elongation of **NP5H** to **NP6H** and **NP7H** should result in even larger and more selective chiroptical responses.

Results and discussion

Synthesis of NP4H, NP5H and NP5H-iso. We built the synthetic design of **NP4H** and **NP5H** upon several previous discoveries: acene-linked PDI derivatives undergo regioselective intramolecular oxidative/eliminative photocyclization at the *peri* position;[18,19] and an inside-out strategy proved crucial in the successful assembly of **NP3H**, in which a simple core structure (e.g., **1** to **2** to **NP4H**, Figure 2a) was expanded progressively, as opposed to fusing extended PDI subunits to the central core in the late stage of the synthesis (e.g., **5** to **NP5H-iso**, Figure 2b).[18b] In addition, we utilized the C2-symmetric nature of **NP4H** and **NP5H** in the synthesis, which afford such long helicenes in relatively few steps (Figure 2). This highly modular and efficient approach will also be useful in accessing the higher order oligomers and PDI helicenes with other arene linkers.

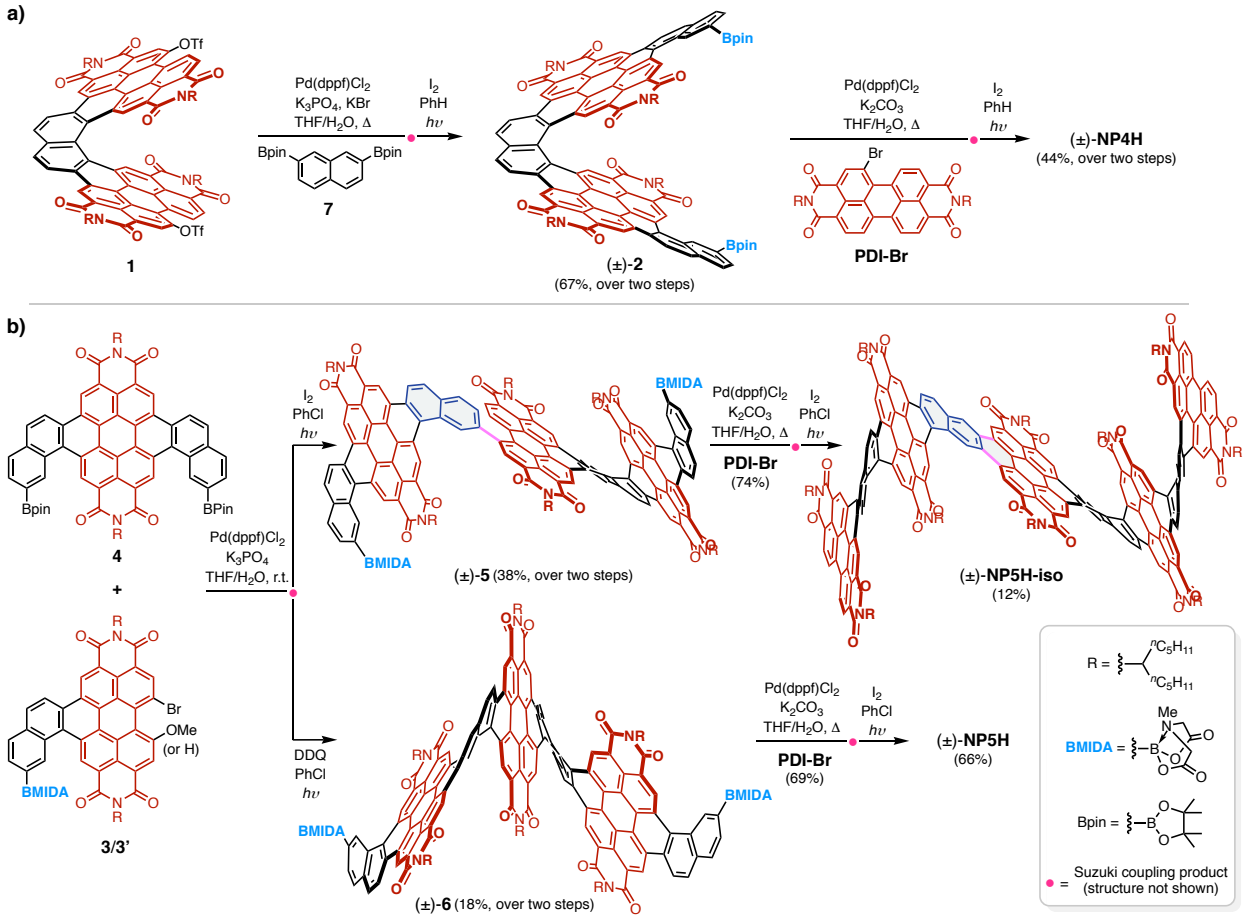

Figure 2. a) Synthesis of **NP4H** via two Suzuki-Miyaura cross-coupling/photocyclization sequences from bis-triflate **1**. b) Different photocyclization conditions led to the syntheses of **NP5H-iso** and **NP5H** from the same starting materials. More details are available in Supporting Information Section III.

The synthesis of **NP4H** (Figure 2a) commenced with the preparation of bis-pinacol boronates (Bpin) substituted helicene **2** from bis-triflated helicene **1** (see Supporting Information Section III for synthetic details) and 2,7-diBpin naphthalene **7** via a two-fold Suzuki-Miyaura cross-coupling/regioselective photocyclization sequence. Subsequent coupling between **2** and **PDI-Br** and the final visible-light induced cyclization in the presence of stoichiometric iodine provided **NP4H** in good yield.

In the route to **NP5H**, *N*-methyliminodiacetic acid (MIDA) boronate esters were used to serve as masked aryl boronic acids for iterative Suzuki-Miyaura cross-couplings.[20,21] Namely, a two-fold chemoselective cross-coupling of aryl bromide **3** and bis-Bpin **4**, in which the MIDA functional group within **3** remained intact, followed by two photocyclization events furnished the core building block bis-MIDA boronate **6** (Figure 2b). Interestingly, an unexpected reduction occurred under the typical photocyclization conditions. This reduction led to the formation of a ring-opened product **5** as the dominant product, which failed to convert further into **6** even at high temperatures (see Supporting Information page S18, and Figure S7 for more discussions). We found that the presence of 2,3-dichloro-5,6-dicyano-1,4-benzoquinone (DDQ) in the photocyclization mitigates this net reduction to produce **6** as the major product. Nonetheless, we first proceeded with **5** in the cross-coupling reaction with **PDI-Br**, after which three individual photocyclization are required to afford **NP5H**. However, we obtained the less sterically congested isomer **NP5H-iso** (see Figure S8 for DFT-optimized structure) from this route. On the other hand, following the installation of two PDI units on **6**, **NP5H** was obtained smoothly by the standard photocyclization. This once again underlines the importance of an inside-out strategy in which the overall strain in longer PDI-helicenes is distributed more evenly to each cyclization reaction.

The C2 symmetry of **NP4H** and **NP5H** is evident in their ^{1}H NMR spectra, whereas every aromatic proton resonance is unique in the spectrum of **NP5H-iso** due to its lack of symmetry. Despite their sizes, both **NP4H**, **NP5H**, and **NP5H-iso** readily dissolve in common organic solvents, such as dichloromethane, toluene, and tetrahydrofuran, making them suitable for further investigations and potential applications because of their solution processability.

Chiroptical Properties. We resolved racemic **NP4H**, **NP5H**, and **NP5H-iso** by chiral high-performance liquid chromatography (Figure S4) and measured the ECD (Figure 3). As expected, the chiroptical response is greater in the longer oligomers of the **NPnH** series for essentially every transition (Figure S6). Compared to **NPDH** (Figure S3a), in which only one [6]helicene unit is present, the chiroptical properties are greatly amplified in **NP4H** and **NP5H**. The bisignate feature centered at ca. 400 nm—characteristic of exciton coupled ECD—is uniformly the largest Cotton effect for each molecule in the **NPnH** (n > 2) series as well as **NP5H-iso**. Particularly, the largest ECD of **NP5H** ($|\Delta\varepsilon|_{max}$ of 1920 M^{-1} cm^{-1} at 420 nm) in the visible spectrum is higher than that of any reported discrete molecule.[16] This ECD band increases 1.7-fold from **NP4H** (1100 M^{-1} cm^{-1} at 410 nm) to **NP5H**, larger than the 1.3-fold increase from **NP3H** (820 M^{-1} cm^{-1} at 410 nm) to **NP4H**. Moreover, **NP5H** has a local maximum $|\Delta\varepsilon|$ of 820 M^{-1} cm^{-1} at 550 nm, and such strong ECD in the longer wavelengths has rarely been observed.[16b,22] This region also represents the most noticeable difference in ECD across the **NPnH** series: the $|\Delta\varepsilon_{550nm}|$ of **NP5H** is 2.5 and 6.6 times larger than the $|\Delta\varepsilon|$ of **NP4H** (320 M^{-1} cm^{-1}) and **NP3H** (120 M^{-1} cm^{-1}) at ca. 540 nm, respectively. **NP4H** and **NP5H** also preferentially absorb only one hand of polarized light over a wide range of the visible spectrum (ca. 400–580 nm).

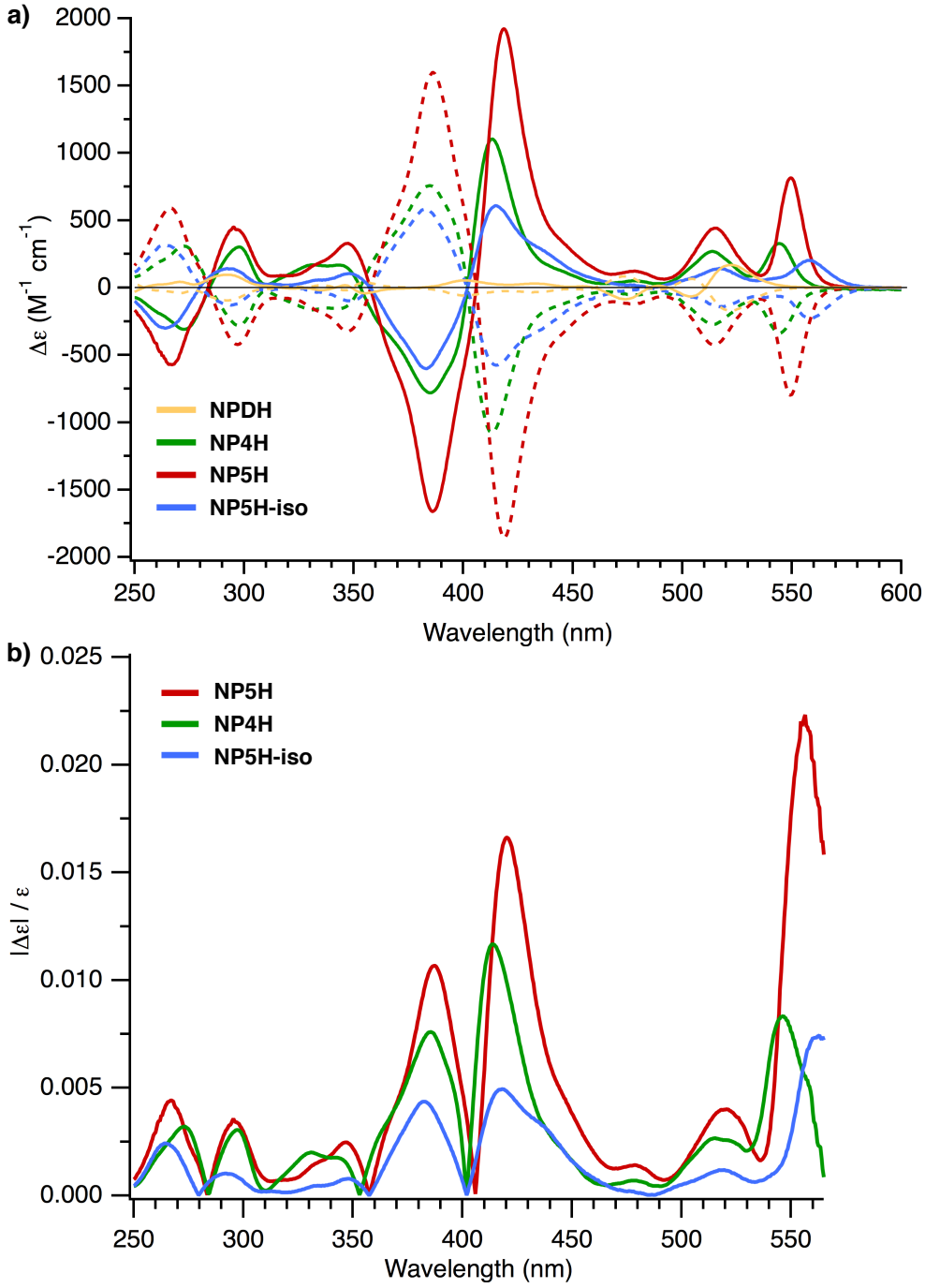

Figure 3. a) The ECD spectra of **NP4H**, **NP5H** and **NP5H-iso** measured in THF (10^{-6} M, 1 cm path length) at ambient temperature. b) The comparison of anisotropy factors between **NP4H**, **NP5H** and **NP5H-iso**.

The difference in ECD intensity between **NP5H** and **NP5H-iso** is also noteworthy. Although they both consist of five PDI units, perturbed symmetry in the latter structure would be disadvantageous for exciton-like interactions as a consequence of each PDI (red, Figure 1) and carbo[6]helicene (grey, Figure 1) being unique. Indeed, the ECD of **NP5H** overwhelms that of **NP5H-iso** (Figure 3a): the $|\Delta\varepsilon|_{max}$ of **NP5H** is 3.1 times greater than the $|\Delta\varepsilon|_{max}$ of **NP5H-iso** (610 M^{-1} cm^{-1}) at ca. 410 nm (i.e., the wavelength of their largest ECD); and a 3.9-fold disparity can be observed

for the Cotton effect at the highest wavelength (820 M^{-1} cm^{-1} at 550 nm vs 210 M^{-1} cm^{-1} at 560 nm). Intriguingly, the overall ECD of **NP5H-iso** is also smaller than that of **NP3H** (Figure S6), even though **NP5H-iso** formally is comprised of **NP3H** and **NPDH** units, which are covalently linked by a central naphthalene (shown in blue in Figure 1). The important conclusion is that a small structural defect in a helicene that discontinues the helical symmetry can substantially impair its ECD. Therefore, atomic precision—especially a challenge in polymeric and supramolecular systems—is critical in the design and synthesis of high-performance chiroptical materials.

The more intense ECD of **NP5H** does not simply correlate with larger molar absorptivity (Figure S5). The pentameric PDI helicenes have slightly higher molar absorptivities than that of **NP4H** (e.g., ~1.25×10^5 M^{-1} cm^{-1} vs ~1.0×10^5 M^{-1} cm^{-1} at ~510 nm), which may simply be attributed to more PDI units in the molecule (i.e., 5 versus 4), but the increase is minor relative to their ECD disparities. Moreover, the difference in their dissymmetry factors for the largest Cotton effect at 400–420 nm of each **NPnH** and **NP5H-iso** is obvious (Figure 3b). This $|\Delta\varepsilon|/\varepsilon$ value progresses almost linearly from **NP3H** (0. 9%) to **NP4H** (1.2%) to **NP5H** (1.7%), which is considerably greater than that of **NP5H-iso** (0.5%). Once again, the most noticeable difference is manifest in the lowest energy band: the anisotropy factor of **NP5H** at 550 nm ($|\Delta\varepsilon|/\varepsilon$ of 2.2%) is the highest among all reported PDI-helicenes,[14c-d,16g,18,23,24] which nearly triples the peak values of **NP4H** (0.8%) and **NP5H-iso** (0.7%), and sextuples that of **NP3H** (0.4%) at ca. 540 nm.

The photoluminescence quantum yields (Φ) of **NP4H** and **NP5H** measured in THF at ambient temperatures are 58% and 68%, respectively, which are superior to many other helicene structures, including **NPDH** (27%) and **NP3H** (44%).[18] Rigidity in polyaromatics often thwarts non-radiative decay by impeding the structural reorganization in the excited state and thus promotes fluorescence.[25] Indeed, the Φ of the less rigid **NP5H-iso (**Figure S8) is 37%, considerably lower than that of **NP5H**. It is worth noting that the **NPnH** series is a rare showcase of enhancing both chiroptical properties and quantum yields as the length of the helix increases (Figures S3 and S6). For the carbo[n]helicenes, the rate of intersystem crossing increases with more *ortho*-fused benzene rings, resulting in decreased fluorescence quantum yield, and the fusion of multiple carbohelicenes hardly enhances both properties[11]. The trend we identified here may also be applicable to analogous PDI helicenes with different aromatic linkers, which could lead to future design of other attractive chiroptical materials.[18,23,24]

Single crystal X-ray diffraction analysis. In spite of such structural complexity, crystals of racemic **NP5H** suitable for X-ray diffraction analysis were obtained (see Supporting Information Section V for details). In the solid state, the same exact helicene architecture (e.g., M1, red, Figure 4a) constitutes a supramolecular chiral column along the y axis with an intermolecular π-π stacking of ca. 3.4 Å (Figure 4b). The asymmetric unit contains two helices with the same chirality that screw to each other, resulting in a close contact between their nearest atoms in the backbone (ca. 3.3 Å, Figure 4a). The helicene skeleton of **NP5H** is extremely compact, even more so than **NP3H**:[18b] the carbon-to-carbon distance between adjacent PDI subunits can be as short as ca. 2.8 Å, greatly shorter than the sum of the van der Waals radius of two carbon atoms (3.4 Å). The extensive overlap between the PDI π-surfaces precludes the formation of other potential stereoisomers during the synthesis at high temperature (Figure S4). Still, the helix of **NP5H** covers a long length (ca. 1.9 nm), measured between the cores of the terminal PDI moieties. The g-factor of

supramolecular multi-helicenes has been computed to be dependent largely on the specific mutual orientation between the coupled chromophores while less sensitive to the inter-helicene distance[11]. The considerable amplification of ECD and dissymmetry (|Δε|/ε) for **NP4H** and **NP5H** relative to **NPDH** and **NP3H** further supports that couplings between each important subunit (i.e., [6]helicene and PDI) remains effective in these long helicenes.

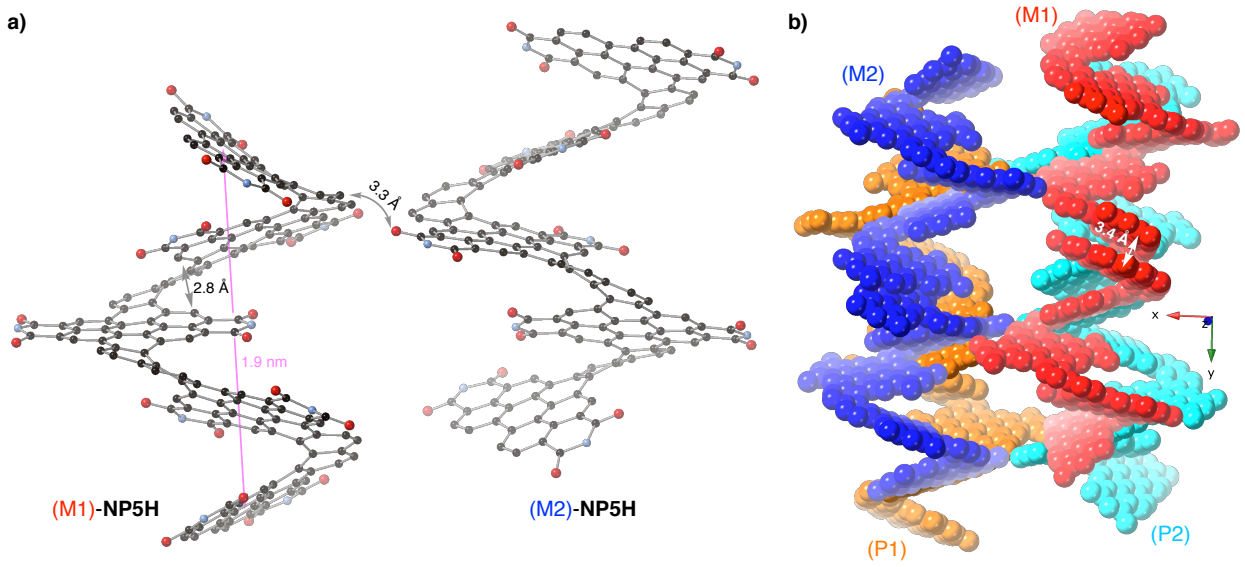

Figure 4. Single crystal X-ray diffraction analysis of racemic **NP5H.** a) two molecules of **NP5H** with the same chirality [two left-handed, (M1)- and (M2)-**NP5H**, are shown] are present in the asymmetric unit. b) Crystal packing of racemic **NP5H**. (M1)/(P1) and (M2)/(P2) are both a pair of enantiomers. Only non-hydrogen atoms are shown and the alkyl groups are omitted for clarity.

Computational analysis. We used TD-DFT to simulate and interpret the absorption and ECD spectra of **NP4H** and **NP5H**, adopting the CAM-B3LYP/6-31+G(d,p) level of theory (Figure 5, see Supporting Information page S71 for details).[26] The calculations reproduce the general shape of the ECD and the absorption, allowing us to assign the spectra characterized by a negative band at λ>500 nm and a strong negative/positive bisignate feature at ca. 400 nm to the enantiomers with M helicity. In addition, the calculations nicely capture the enhancement of the ECD intensity from **NP4H** to **NP5H**. Since we scaled the absorption and ECD intensities by the same factor, the calculated dissymmetry factor also agrees with the experimental data. To account for vibronic effects, we also report absorption and the emission spectra computed at vibronic level with the code FCclasses 3.0 (Figures S14 and S26), which show further improved accuracies and a nice reproduction of the shape of the emission line.

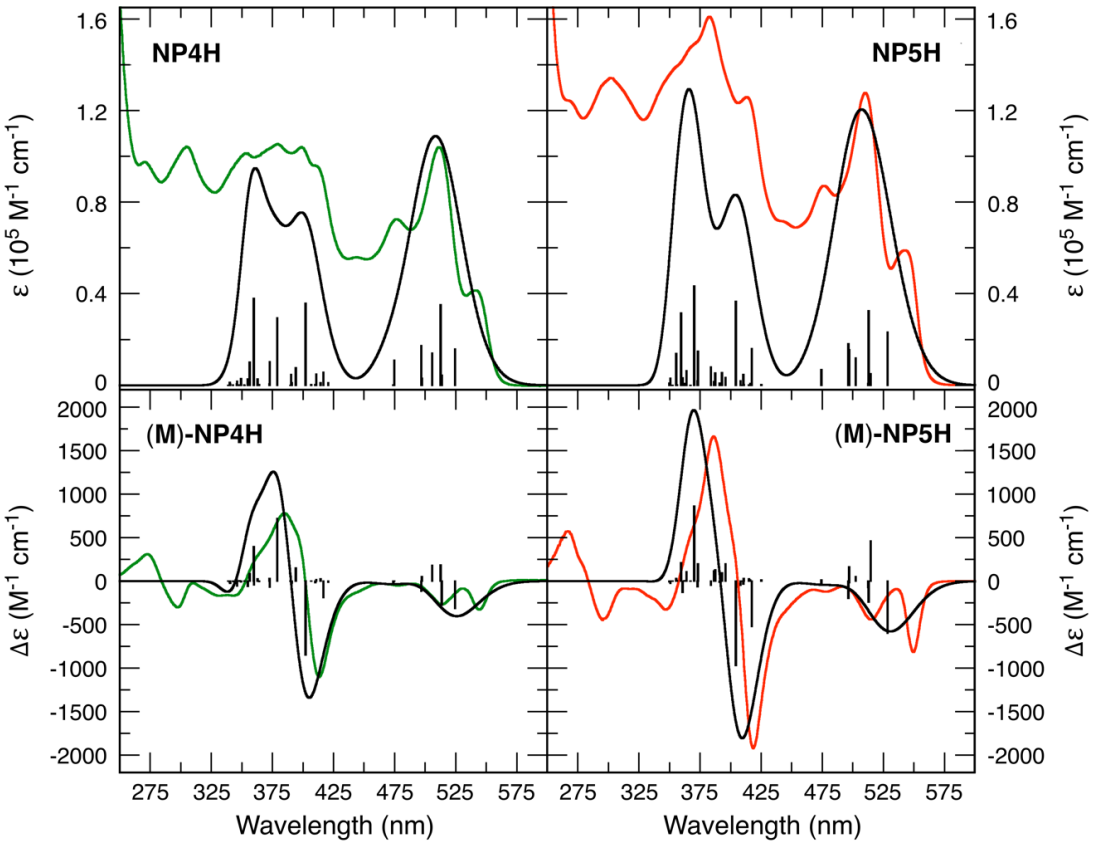

Figure 5. Comparison of the computed (black) and experimental (colored) absorption and ECD spectra. The data for **NP4H** (left) and **NP5H** (right) are computed at the CAM-B3LYP/6-31+G(d,p) level of theory in the gas phase. Sticks show the contribution of the different electronic states. Convoluted spectra were obtained by attaching to each stick a Gaussian linewidth with half width at half maximum (HWHM) of 0.1 eV. Computed spectra are red-shifted by 0.46 eV and their intensity are scaled by a factor of 0.48.

The agreement between computational and experimental spectra validates the use of TD-DFT to investigate the nature of the excited states responsible for the main ECD. The properties of these states together with the corresponding transition electric and magnetic dipoles in the **NPnH** series (n=3 to 7) are reported in Tables S2–S4. The analysis of the electronic transitions between Kohn-Sham Molecular Orbitals (MOs) is very complicated, because each excited state is made up by several different transitions and the involved MOs are in general spread on most of the molecular structure (Figure S17). Therefore here we present an alternative analysis, based on the difference of their electronic densities (DeD) with respect to the ground state. DeD allows us to to monitor where the electronic density changes as a consequence of the excitation. Based on the DeD analysis of the corresponding states of **NP4H** and **NP5H** (Figures S18 and S20), the electronic states for the low-energy band at 500 nm, where their ECD intensities and g-factors differ the most, are mainly localized on the PDI units. On the other hand, the bisignated feature at 400 nm is due to the coupling of states localized essentially on the carbo[6]helicenes (grey, Figure 1) in **(M)-NP4H** and **(M)-NP5H** (Figures S22–S24), although, due to the dimension of the molecule and the number of excited states, the picture is more complex than **(M)-NP3H**. The origin of the ECD couplet at 400 nm is further supported by the predictions for two model systems, in which only the five PDI fragments (PDI_5) or the carbohelicenes in the **(M)-NP5H** structure are

considered, respectively (Figure S25). The same large ECD feature exists in the computed spectrum of the carbohelicene fragments but not in that of PDI_5.

In summary, these analyses suggest the strong enhancement of the bisignate feature at ca. 400 nm arises from exciton-like interactions of states localized on these idealized carbo[6]helicenes units. Additionally, here we show that the negative bands at λ>500 nm, which intensify drastically from **NP3H** to **NP5H**, arise from exciton-like couplings of the PDI fragments. Notably, the absolute rotatory strengths of certain states responsible for the ECD at these wavelengths are comparable to those giving rise to the ECD couplet at 400 nm. However, at λ>500 nm, states with positive and negative contributions are much closer in energy, which prevents the occurrence of a bisignate feature in the ECD and leads to a partial quenching of the signal.

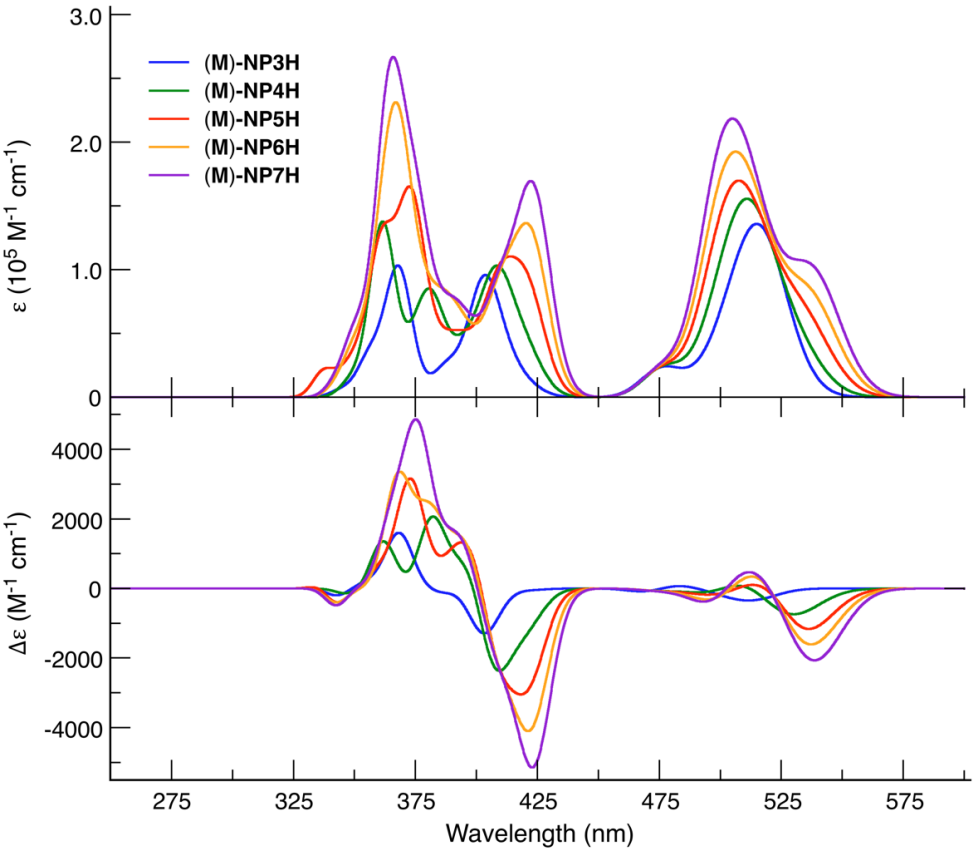

Figure 6. Predicted electronic absorption (top) and CD (bottom) spectra of **(M)-NPnH** (n=3,4,5,6,7). All stick transitions were convoluted with a Gaussian function of HWHM = 0.1 eV. Spectra were red-shifted by 0.53 eV and scaled by a factor 0.48.

Finally, we utilized computational modeling to predict the behavior of longer members of the **NPnH** series**.** Figure 6 shows the computed absorption and ECD spectra of the **NPnH** series from n = 3 to 7, adopting 6-31G(d) for convenience, a smaller basis set that however only causes a small blue-shift (Figure S30). Calculations predict that both the ECD band at λ>500 nm and the bisignate feature at ca. 400 nm are further enhanced in **NP6H** and even more in **NP7H**, suggesting the exciton-like interactions can persist over such long distances. Moreover, the g-factor also increases as the helical axis lengthens. The simulated spectra of the longer members exhibit a more pronounced red-

wing shoulder in the lowest energy band. Such band is due to the lowest-energy state S1 that, in our calculations, gets progressively more separated from the higher-lying states at the increase of *n*. In short, **NP6H** and **NP7H** are predicted to show greater chiroptical activities than **NP5H**, and therefore, they are potentially even better candidates for chiral optoelectronics. Synthetic efforts towards these longer nanoribbons are currently ongoing in our laboratory.

Conclusion

In conclusion, we have synthesized and studied two long and enantiomerically stable helicenes named **NP4H** and **NP5H** with exceptional ECD responses, which also serve as a platform for understanding the mechanism of chiral amplification in helicenoids. In particular, **NP5H** shows the largest ECD ($|\Delta\varepsilon|_{max}$ of 1920 M^{-1} cm^{-1} at 420 nm) in the visible range of any discrete molecule. The comparison of the g-factor among the **NPnH** series clearly suggests that the intense ECD does not stem from increased absorbance: **NP5H** also exhibits larger g-factors (up to 2.2%) than the shorter analogues. The outstanding chiroptical properties, large molar absorptivity, and high fluorescence quantum yield of **NP5H** demonstrate its potential as a material candidate for chiral optoelectronics. Theoretical calculations provide additional insights to the mechanism of the amplified ECD: interactions of states localized on the PDI units, and on the carbo[6]helicene fragments are responsible for the main ECD increase at >500 nm and 400 nm, respectively. Finally, this work can serve as a foundation for the design of new chiroptical materials with enhanced and/or complementary properties: chiroptical activities are predicted to be further amplified in higher oligomers (i.e., **NP6H**, **NP7H**, etc.); this trend might also be applicable to analogous helical nanoribbons with other arene spacers between each PDI.

Associated Content

Supporting Information

The Supporting Information is available free of charge at https://pubs.acs.org/doi.

Synthetic details and characterization, supporting Figures, and theoretical details (PDF)

checkCIF/PLATON report (PDF)

X-ray crystallographic data for **NP5H** (CIF)

Author Information

Corresponding Authors

Fabrizio Santoro (fabrizio.santoro@pi.iccom.cnr.it), Nathaniel J. Schuster (njs2154@columbia.edu), and Colin Nuckolls (cn37@columbia.edu)

Notes

The authors declare no competing financial interests.

Acknowledgements

C.N. thanks Sheldon and Dorothea Buckler for their generous support. Support for this research was provided by the U.S. Office of Naval Research under award No. N00014-16-1-2921 and the U.S. Department of Energy, Office of Science, Office of Basic Energy Sciences, under award No. DE-SC0014563 and No. DE-SC0019440. D.A. acknowledges Fundación Ramón Areces (Spain) for its support. S.K.P. and M.P. appreciate the support from the Danish Council for Independent Research (DFF 4181-00206 and 9040-00265) and from the University of Copenhagen. The ECD spectra were recorded at the Precision Biomolecular Characterization Facility (PBCF) at

Columbia University. Essential instrumentation in the PBCF was made possible by funding from the U.S. National Institutes of Health under award no. S10OD025102. We thank Dr. Jia Ma (Columbia) for his management of the PBCF. We appreciate the Owen laboratory at Columbia University for assistance in quantum yield measurements. SCXRD was performed at the Shared Materials Characterization Laboratory (SMCL) at Columbia University. We thank Dr. Daniel Paley (Columbia) for assistance in structural refinement. Use of the SMCL was made possible by funding from Columbia University.

References

1. (a) Gingras, M. One Hundred Years of Helicene Chemistry. Part 1: Non-Stereoselective Syntheses of Carbohelicenes. *Chem. Soc. Rev.* **2013**, *42*, 968–1006. (b) Gingras, M.; Félix, G.; Peresutti, R. One Hundred Years of Helicene Chemistry. Part 2: Stereoselective Syntheses and Chiral Separations of Carbohelicenes. *Chem. Soc. Rev.* **2013**, *42*, 1007–1050. (c) Gingras, G. One Hundred Years of Helicene Chemistry. Part 3: Applications and Properties of Carbohelicenes. *Chem. Soc. Rev.* **2013**, *42*, 1051–1095. (d) Shen, Y.; Chen, C. F. Helicenes: Synthesis and Applications. *Chem. Rev*. **2012**, *112*, 1463–1535.
2. Aillard, P.; Voituriez, A.; Marinetti, A. Helicene-like Chiral Auxiliaries in Asymmetric Catalysis. *Dalt. Trans.* **2014**, *43*, 15263–15278.
3. (a) Isla, H.; Crassous, J. Helicene-Based Chiroptical Switches. *C. R. Chim.* **2016**, *19*, 39–49. (b) Kalachyova, Y.; Guselnikova, O.; Elashnikov, R.; Panov, I.; Žádný, J.; Církva, V.; Storch, J.; Sykora, J.; Zaruba, K.; Švorčík, V.; Lyutakov, O. Helicene-SPP-Based Chiral Plasmonic Hybrid Structure: Toward Direct Enantiomers SERS Discrimination. *ACS Appl. Mater. Interfaces* **2019**, *11*, 1555–1562.
4. Verbiest, T.; Van Elshocht, S.; Kauranen, M.; Hellemans, L.; Snauwaert, J.; Nuckolls, C.; Katz, T. J.; Persoons, A. Strong Enhancement of Nonlinear Optical Properties through Supramolecular Chirality. *Science* **1998**, *282*, 913–915.
5. Kiran, V.; Mathew, S. P.; Cohen, S. R.; Hernández Delgado, I.; Lacour, J.; Naaman, R. Helicenes - A New Class of Organic Spin Filter. *Adv. Mater.* **2016**, *28*, 1957–1962.
6. (a) Brandt, J. R.; Salerno, F.; Fuchter, M. J. The Added Value of Small-Molecule Chirality in Technological Applications. *Nat. Rev. Chem.* **2017**, *1*, 45. (b) Pop, F.; Zigon, N.; Avarvari, N. Main-Group-Based Electro- And Photoactive Chiral Materials. *Chem. Rev.* **2019**, *119*, 8435–8478.
7. Majewski, M. A.; Stępień, M. Bowls, Hoops, and Saddles: Synthetic Approaches to Curved Aromatic Molecules. *Angew. Chem. Int. Ed.* **2019**, *58*, 86–116.
8. (a) Mori, K.; Murase, T.; Fujita, M. One-Step Synthesis of [16]Helicene. *Angew. Chem. Int. Ed.* **2015**, *54*, 6847–6851. (b) Nakakuki, Y.; Hirose, T.; Sotome, H.; Miyasaka, H.; Matsuda, K. Hexa- Peri - Hexabenzo[7]Helicene: Homogeneously π-Extended Helicene as a Primary Substructure of Helically Twisted Chiral Graphenes. *J. Am. Chem. Soc.* **2018**, *140*, 4317–4326. (c) Evans, P. J.; Ouyang, J.; Favereau, L.; Crassous, J.; Fernández, I.; Perles, J.; Martín, N. Synthesis of a Helical Bilayer Nanographene. *Angew. Chem. Int. Ed.* **2018**, *57*, 6774–6779. (d) Fernández-García, J. M.; Evans, P. J.; Medina Rivero, S.; Fernández, I.; García-Fresnadillo, D.; Perles, J.; Casado, J.; Martín, N. π-Extended Corannulene-Based Nanographenes: Selective Formation of Negative Curvature. *J. Am. Chem. Soc.* **2018**, *140*, 17188–17196. (e) Cruz, C. M.; Castro-Fernández, S.; Maçôas, E.; Cuerva, J. M.; Campaña, A. G. Undecabenzo[7]Superhelicene: A Helical Nanographene Ribbon as a Circularly Polarized Luminescence Emitter. *Angew. Chem. Int. Ed.* **2018**, *57*, 14782–14786. (f) Kiel, G. R.; Patel, S. C.; Smith, P. W.; Levine, D. S.; Tilley, T. D. Expanded Helicenes: A General Synthetic Strategy and Remarkable Supramolecular and Solid-State Behavior. *J. Am. Chem. Soc.* **2017**, *139*, 18456–18459. (g) Nakakuki, Y.; Hirose, T.; Matsuda, K. Synthesis of a Helical Analogue of Kekulene: A Flexible π-Expanded Helicene with Large Helical Diameter Acting as a Soft Molecular Spring. *J. Am. Chem. Soc.* **2018**, *140*, 15461–15469.
9. (a) OuYang, J.; Crassous, J. Chiral Multifunctional Molecules Based on Organometallic Helicenes: Recent Advances. *Coord. Chem. Rev.* **2018**, *376*, 533–547. (b) Dhbaibi, K.; Favereau, L.; Crassous, J. Enantioenriched Helicenes and Helicenoids Containing Main-Group Elements (B, Si, N, P). *Chem. Rev.* **2019**, *119*, 8846–8953. (c) Nejedlý, J.; Šámal, M.; Rybáček, J.; Tobrmanová, M.; Szydlo, F.; Coudret, C.; Neumeier, M.; Vacek, J.; Vacek Chocholoušová, J.; Buděšínský, M.; Šaman, D.; Bednárová, L.; Sieger, L.; Stará, I. G.; Starý, I. Synthesis of Long Oxahelicenes by Polycyclization in a Flow Reactor. *Angew. Chem. Int. Ed.* **2017**, *56*, 5839–5843. (d) Fujikawa, T.; Segawa, Y.; Itami, K. Laterally π-Extended Dithia[6]Helicenes with Heptagons: Saddle-

Helix Hybrid Molecules. *J. Org. Chem.* **2017**, *82*, 7745–7749. (e) Nakamura, K.; Furumi, S.; Takeuchi, M.; Shibuya, T.; Tanaka, K. Enantioselective Synthesis and Enhanced Circularly Polarized Luminescence of S-Shaped Double Azahelicenes. *J. Am. Chem. Soc.* **2014**, *136*, 5555–5558. (f) Kato, K.; Furukawa, K.; Mori, T.; Osuka, A. Porphyrin-Based Air-Stable Helical Radicals. *Chem. Eur. J.* **2018**, *24*, 572–575.

10. Berova, N.; Nakanishi, K.; Woody, R. W. *Circular Dichroism: Principles and Applications*; John Wiley & Sons, 2000.
11. Tanaka, H.; Ikenosako, M.; Kato, Y.; Fujiki, M.; Inoue, Y.; Mori, T. Symmetry-Based Rational Design for Boosting Chiroptical Responses. *Commun. Chem.* **2018**, *1*, 38.
12. Nakai, Y.; Mori, T.; Inoue, Y. Theoretical and Experimental Studies on Circular Dichroism of Carbo[n]Helicenes. *J. Phys. Chem. A* **2012**, *116*, 7372–7385.
13. Li, C.; Yang, Y.; Miao, Q. Recent Progress in Chemistry of Multiple Helicenes. *Chem. Asian J.* **2018**, *13*, 884–894.
14. (a) Berezhnaia, V.; Roy, M.; Vanthuyne, N.; Villa, M.; Naubron, J. V.; Rodriguez, J.; Coquerel, Y.; Gingras, M. Chiral Nanographene Propeller Embedding Six Enantiomerically Stable [5]Helicene Units. *J. Am. Chem. Soc.* **2017**, *139*, 18508–18511. (b) Zhu, Y.; Xia, Z.; Cai, Z.; Yuan, Z.; Jiang, N.; Li, T.; Wang, Y.; Guo, X.; Li, Z.; Ma, S.; Zhong, D.; Li, Y.; Wang, J. Synthesis and Characterization of Hexapole [7]Helicene, A Circularly Twisted Chiral Nanographene. *J. Am. Chem. Soc.* **2018**, *140*, 4222–4226. (c) Liu, G.; Koch, T.; Li, Y.; Doltsinis, N. L.; Wang, Z. Nanographene Imides Featuring Dual-Core Sixfold [5]Helicenes. *Angew. Chem. Int. Ed.* **2019**, *58*, 178–183. (d) Meng, D.; Liu, G.; Xiao, C.; Shi, Y.; Zhang, L.; Jiang, L.; Baldridge, K. K.; Li, Y.; Siegel, J. S.; Wang, Z. Corannurylene Pentapetalae. *J. Am. Chem. Soc.* **2019**, *141*, 5402–5408. (e) Cruz, C. M.; Márquez, I. R.; Castro-Fernández, S.; Cuerva, J. M.; Maçôas, E.; Campaña, A. G. A Triskelion-Shaped Saddle–Helix Hybrid Nanographene. *Angew. Chem. Int. Ed.* **2019**, *58*, 8068–8072. (f) Roy, M.; Berezhnaia, V.; Villa, M.; Vanthuyne, N.; Giorgi, M.; Naubron, J. V.; Poyer, S.; Monnier, V.; Charles, L.; Carissan, Y.; Hagebaum-Reignier, D.; Rodriguez, J.; Gingras, M.; Coquerel, Y. Stereoselective Syntheses, Structures, and Properties of Extremely Distorted Chiral Nanographenes Embedding Hextuple Helicenes. *Angew. Chem. Int. Ed.* **2020**, *59*, 3264–3271.
15. Würthner, F.; Saha-Möller, C. R.; Fimmel, B.; Ogi, S.; Leowanawat, P.; Schmidt, D. Perylene Bisimide Dye Assemblies as Archetype Functional Supramolecular Materials. *Chem. Rev.* **2016**, *116*, 962–1052.
16. (a) Zhu, Y.; Guo, X.; Li, Y.; Wang, J. Fusing of Seven HBCs Toward a Green Nanographene Propeller. *J. Am. Chem. Soc.* **2019**, *141*, 5511–5517. (b) Werner, A.; Michels, M.; Zander, L.; Lex, J.; Vogel, E. 'Figure Eight' Cyclooctapyrroles: Enantiomeric Separation and Determination of the Absolute Configuration of a Binuclear Metal Complex. *Angew. Chem. Int. Ed.* **1999**, *38*, 3650–3653. (c) Sugiura, H.; Nigorikawa, Y.; Saiki, Y.; Nakamura, K.; Yamaguchi, M. Marked Effect of Aromatic Solvent on Unfolding Rate of Helical Ethynylhelicene Oligomer. *J. Am. Chem. Soc.* **2004**, *126*, 14858–14864. (d) Brahma, S.; Ikbal, S. A.; Dhamija, A.; Rath, S. P. Highly Enhanced Bisignate Circular Dichroism of Ferrocene-Bridged Zn(II) Bisporphyrin Tweezer with Extended Chiral Substrates Due to Well-Matched Host-Guest System. *Inorg. Chem.* **2014**, *53*, 2381–2395. (e) Sato, S.; Yoshii, A.; Takahashi, S.; Furumi, S.; Takeuchi, M.; Isobe, H. Chiral Intertwined Spirals and Magnetic Transition Dipole Moments Dictated by Cylinder Helicity. *Proc. Natl. Acad. Sci. U. S. A.* **2017**, *114*, 13097–13101. (f) Wang, J.; Zhuang, G.; Chen, M.; Lu, D.; Li, Z.; Huang, Q.; Jia, H.; Cui, S.; Shao, X.; Yang, S.; Du, P. Selective Synthesis of Conjugated Chiral Macrocycles: Sidewall Segments of (−)/(+)-(12,4) Carbon Nanotubes with Strong Circularly Polarized Luminescence. *Angew. Chem. Int. Ed.* **2020**, *59*, 1619–1626. (g) Schuster, N. J.; Joyce, L. A.; Paley, D. W.; Ng, F.; Steigerwald, M. L.; Nuckolls, C. The Structural Origins of Intense Circular Dichroism in a Waggling Helicene Nanoribbon. *J. Am. Chem. Soc.* **2020**, *142*, 7066–7074.
17. Pescitelli, G.; Di Bari, L.; Berova, N. Application of Electronic Circular Dichroism in the Study of Supramolecular Systems. *Chem. Soc. Rev.* **2014**, *43*, 5211–5233.
18. (a) Schuster, N. J.; Paley, D. W.; Jockusch, S.; Ng, F.; Steigerwald, M. L.; Nuckolls, C. Electron Delocalization in Perylene Diimide Helicenes. *Angew. Chem. Int. Ed.* **2016**, *55*, 13519–13523. (b) Schuster, N. J.; Hernández Sánchez, R.; Bukharina, D.; Kotov, N. A.; Berova, N.; Ng, F.; Steigerwald, M. L.; Nuckolls, C. A Helicene Nanoribbon with Greatly Amplified Chirality. *J. Am. Chem. Soc.* **2018**, *140*, 6235–6239.
19. Khokhlov, K.; Schuster, N. J.; Ng, F.; Nuckolls, C. Functionalized Helical Building Blocks for Nanoelectronics. *Org. Lett.* **2018**, *20*, 1991–1994.

20. Li, J.; Ballmer, S. G.; Gillis, E. P.; Fujii, S.; Schmidt, M. J.; Palazzolo, A. M. E.; Lehmann, J. W.; Morehouse, G. F.; Burke, M. D. Synthesis of Many Different Types of Organic Small Molecules Using One Automated Process. *Science* **2015**, *347*, 1221–1226.
21. Fyfe, J. W. B.; Valverde, E.; Seath, C. P.; Kennedy, A. R.; Redmond, J. M.; Anderson, N. A.; Watson, A. J. B. Speciation Control during Suzuki-Miyaura Cross-Coupling of Haloaryl and Haloalkenyl MIDA Boronic Esters. *Chem. Eur. J.* **2015**, *21*, 8951–8964.
22. Hsieh, Y. C.; Wu, C. F.; Chen, Y. T.; Fang, C. Te; Wang, C. S.; Li, C. H.; Chen, L. Y.; Cheng, M. J.; Chueh, C. C.; Chou, P. T.; Wang, Y. T. 5,14-Diaryldiindeno[2,1- f:1′,2′ -j]Picene: A New Stable [7]Helicene with a Partial Biradical Character. *J. Am. Chem. Soc.* **2018**, *140*, 14357–14366.
23. Liu, B.; Böckmann, M.; Jiang, W.; Doltsinis, N. L.; Wang, Z. Perylene Diimide-Embedded Double [8]Helicenes. *J. Am. Chem. Soc.* **2020**, *142*, 7092–7099.
24. Milton, M.; Schuster, N. J.; Paley, D. W.; Hernández Sánchez, R.; Ng, F.; Steigerwald, M. L.; Nuckolls, C. Defying Strain in the Synthesis of an Electroactive Bilayer Helicene. *Chem. Sci.* **2019**, *10*, 1029–1034.
25. Berlman, I. *Handbook of Fluorescence Spectra of Aromatic Molecules*, 2nd ed.; Academic Press, Inc.: New York, NY, USA, 1971.
26. Guido, C. A.; Knecht, S.; Kongsted, J.; Mennucci, B. Benchmarking Time-Dependent Density Functional Theory for Excited State Geometries of Organic Molecules in Gas-Phase and in Solution. *J. Chem. Theory Comput.* **2013**, *9*, 2209–2220.

TOC Graphic: